Optical sensing of chlorophyll(in) with dual-spectrum Si LEDs in SOI-CMOS technology

Dutta, Satadal; Steeneken, Peter G.; Verbiest, Gerard J.

DOI
10.1109/JSEN.2021.3086588

Publication date
2022

Document Version
Final published version

Published in
IEEE Sensors Journal

Optical Sensing of Chlorophyll(in) With Dual-Spectrum Si LEDs in SOI-CMOS Technology

Satadal Dutta, Peter G. Steeneken, and Gerard J. Verbiest

***Abstract*—Small and low-cost chlorophyll sensors are popular in agricultural sector and food-quality control. Combining such sensors with silicon CMOS electronics is challenged by the absence of silicon-integrated light-sources. We experimentally achieve optical absorption sensing of chlorophyll based pigments with silicon (Si) micro light-emitting diodes (LED) as light-source, fabricated in a standard SOI-CMOS technology. By driving a Si LED in both forward and avalanche modes of operation, we steer its electroluminescent spectrum between visible (400–900 nm) and near-infrared (~1120 nm). For detection of chlorophyll in solution phase, the dual-spectrum light from the LED propagates vertically through glycerol micro-droplets containing sodium copper chlorophyllin at varying relative concentrations. The transmitted light is detected via an off-chip Si photodiode. The visible to near-infrared color ratio (COR) of the photocurrent yields the effective absorption coefficient. We introduce the LED-specific molar absorption coefficient as a metric to compute the absolute pigment concentration (~0.019 ± 0.006 mol L^{-1}) and validate the results by measurements with a hybrid spectrophotometer. With the same sensor, we also show non-invasive monitoring of chlorophyll in plant leaves. COR sensitivities of ~3.9 x 10^4 $mol^{-1}L$ and ~5.3 x 10^4 $mol^{-1}L$ are obtained for two leaf species, where light from the LED propagates diffusely through the thickness of the leaf prior to detection by the photodiode. Our work demonstrates the feasibility of realizing fully CMOS-integrated optical sensors for biochemical analyses in food sector and plant/human health.**

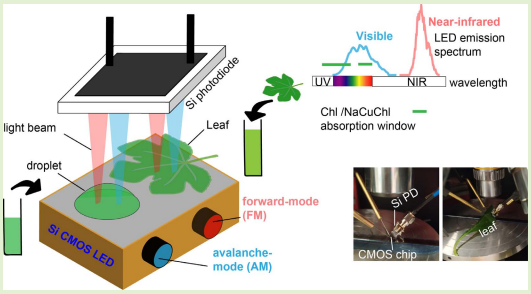

***Index Terms*—Silicon, avalanche breakdown, CMOS, electroluminescence, optical sensor, light-emitting diode, chlorophyll.**

I. Introduction

CHLOROPHYLL (Chl) is an essential pigment for photosynthesis and a key indicator of health of plants [1]. Moreover, chemically stable derivatives of Chl, e.g. chlorophyllins, are key ingredients in a plethora of dietary and medicinal supplements [2]. Sensors to monitor both natural Chl content in leaves and chlorophyllin in food supplements are, thus, widely used in the agricultural sector and for food-quality control [3]–[5]. Optical sensing is highly suitable to detect Chl and its derivatives. This is due to the strong interaction of these pigments with ultraviolet and visible light [6]. While leaf transmittance measurement is popular to monitor Chl non-invasively [7], colorimetric detection of pigments in compact microfluidic systems [8] (and references therein) is becoming popular to ensure fast detection, simple operation and small volume of sample. Advances in semiconductor technology have led to a variety of hybrid light-sources in the same spectral window, e.g. lasers and quasi-monochromatic light-emitting diodes (LEDs), that are employed in the state-of-the-art optical sensors [9], [10]. However, these light-sources are incompatible with silicon (Si) CMOS technology, which is the workhorse for advanced electronic read-out and data processing modules for sensors [11]. This hinders device integration and makes these sensors relatively expensive and bulky.

Silicon photonics is emerging as a key technology for the development of CMOS-integrated optical devices for applications in bio-chemical sensing and data communication links [12]–[19]. Interestingly, Si p-n junction diodes exhibit broad-spectrum electroluminescence (EL) at wavelengths (λ) near 1120 nm in forward mode (FM) and at λ in the range of 400–900 nm in avalanche mode (AM) operation.

Manuscript received May 4, 2021; accepted May 31, 2021. Date of publication June 4, 2021; date of current version June 14, 2022. This work was supported by the Plantenna Research Program and funded by the 4TU Federation, The Netherlands. An earlier version of this article was presented at the 2020 IEEE Sensors Conference and its Proceedings. The associate editor coordinating the review of this article and approving it for publication was Prof. Gijs J. M. Krijnen. *(Corresponding author: Satadal Dutta.)*

The authors are with the Department of Precision and Microsystems Engineering, Delft University of Technology, 2628 Delft, The Netherlands (e-mail: s.dutta-1@tudelft.nl; p.g.steeneken@tudelft.nl; g.j.verbiest@tudelft.nl).

Digital Object Identifier 10.1109/JSEN.2021.3086588

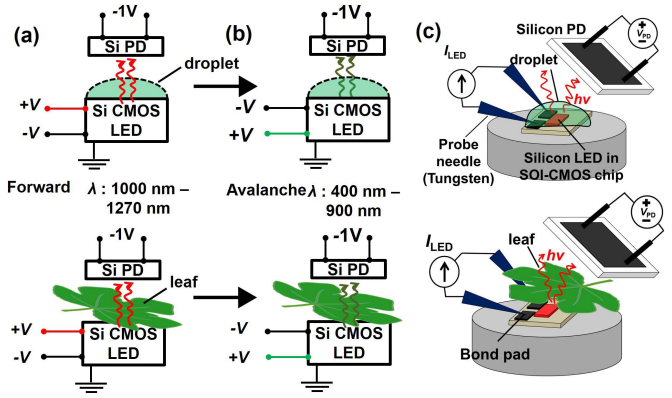

Fig. 1. Schematic block diagram illustrating the optical sensing method. Optical coupling from the Si LED on the CMOS chip to an externally mounted Si PD (reverse biased at 1 V) is measured in presence of a pigmented glycerol droplet (top panel) or a leaf (bottom panel) on top of the LED. The LED is operated in (a) forward mode (FM) and (b) avalanche mode (AM). The pigment (NaCuChl) absorbs light in the range $400 < \lambda < 800$ nm. (c) Schematic of the measurement set-up (not to scale). The on-chip LED is placed on a vacuum chuck and is driven in constant current mode, where electrical probing is done via aluminium bond-pads and tungsten needles. The wavy arrows indicate light propagation.

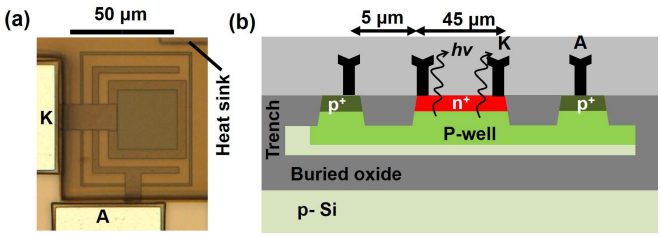

Fig. 2. (a) Top-view micrograph and (b) device cross-section of the n^+p junction LED in a SOI-CMOS technology from NXP Semiconductors [32]. Symbols A and K indicate the anode and cathode terminating in Al bond pads. The LED has a junction area of 45×45 μm^2, and a reverse breakdown voltage of ~17 V.

Although this EL occurs at a low quantum efficiency ($\sim 10^{-3}$–10^{-5}) [20]–[26] due to the indirect bandgap of Si, for many applications the advantages of CMOS integration of the LED outweigh the drawback of low efficiency. Recent advancements [27]–[29] have successfully highlighted the Si LED as a promising candidate for monolithically integrated optical interconnects due to the high responsivity of Si photodiodes (PDs) for wavelengths (λ) < 1000 nm. The ability to electrically switch between visible (VIS) and near-infrared (NIR) emission from a single Si LED eliminates the need for any process modification or device replacement in an optical sensor. In contrast, wavelength tuning in LEDs made of III-V semiconductors require large stoichiometric changes in material composition [30]. The 400 – 1300 nm spectral range is highly suitable for sensing photosynthetic pigments [6], leaf-water status [33], [34], colored contaminants in water [35]–[37] and blood oxygen levels [38].

In this work, we show how Si LEDs fabricated in a standard SOI-CMOS technology are viable light-sources for use in optical absorption sensing systems, by driving a single LED in both FM and AM operation. The emitted light propagates vertically through a pigmented micro-droplet placed on the surface followed by detection by a discrete Si PD mounted externally above the chip (see Fig. 1(a), (b)). We define the color ratio (COR) as ratio of PD photocurrent during AM LED operation to that during FM LED operation. From the COR and the mean height of the droplet (optical path length), we obtain the effective absorption coefficient (α) of the pigmented solution specific to our broadband Si LED. In our recent conference proceedings paper [31], we demonstrated this sensing principle using Carmine pigment. In this paper, we extend our work by sensing Chl-based pigments, namely sodium copper chlorophyllin (NaCuChl) in solution phase and chlorophyll (Chl) in intact plant-leaves.

The rest of the manuscript is organised as follows. Section II describes the experimental device and the method. Sections III-B and III-C present the measurement results and data analyses for sensing with droplets (containing NaCuChl in solution) and with intact leaves (containing naturally occurring Chl.), respectively. Section IV briefly outlines the merits, applicability and future scope of the sensor. Section V summarizes our work.

II. Experimental Set-Up and Method

Fig. 1(c) shows a schematic diagram of the set-up. The on-chip Si LED is placed on a vacuum chuck. The bond-pads are electrically probed by Tungsten needles connected to EverBeing EB-050 micropositioners in a probe station. A BPW34 Si PD from Vishay semiconductors is mounted above the chip at a center-height ~5 mm tilted at ~45 degrees via a micropositioner. The LED is driven in a constant current (sweep) mode and the PD is driven at a fixed reverse bias of 1 V using a Keysight B2912A precision source and measurement unit (SMU). During measurement, either a droplet with NaCuChl. or a leaf is placed on top of the Si LED.

Figs. 2(a) and (b) show, respectively, the optical top-view micrograph (layout), and the schematic device cross-section of the test LED, designed in a standard 130 nm silicon-on-insulator (SOI) CMOS technology [32], from NXP Semiconductors. The LED is a vertical n^+p junction diode with a junction depth of ~0.25 μm, an active junction area of 45×45 μm^2, and an avalanche breakdown voltage of ~17 V [27]. Vertical poly-Si columns are placed near the p-n junction, which connect the SOI layer to the Si substrate. They serve as heat sinks to reduce the thermal resistance significantly.

In a first experiment, we test the sensing principle using droplets containing NaCuChl. A commercially available solution (~10 mM) of NaCuChl (E141), from PipingRock Health Products, LLC. is used as a target. We choose glycerol as the solvent for the droplets. This choice is motivated by its negligible volatility at 300 K, optical transparency for λ in the range 400–1200 nm, and chemical inertness to the SiO_2 layer on the chip surface. We denote the NaCuChl. concentration of the target solution as c_{ref}. This solution is diluted in appropriate volumes of excess glycerol to yield solution specimens of the following relative concentrations (c/c_{ref}) of C1 = 1.0 %,

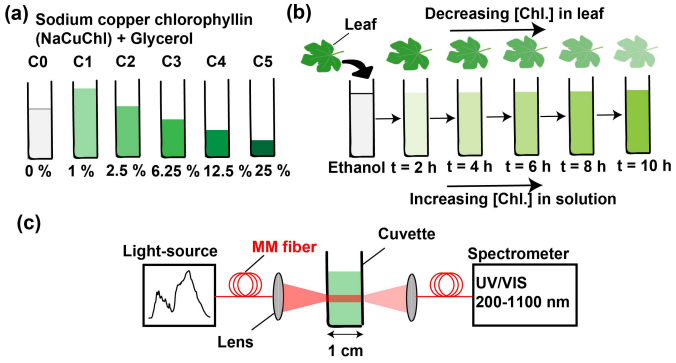

Fig. 3. (a) Solution specimens of sodium copper chlorophyllin (NaCuChl) diluted in laboratory-grade glycerol with indicated concentrations (% by volume) relative to a reference commercial solution (~10 mM) of NaCuChl (E141) in glycerol and water. C0 represents only glycerol. (b) Method for Chl. monitoring in leaves. To emulate chlorophyll deficiency, the test leaf is treated with 12 mL ethanol at 300 K in a graduated vial. At every 2 hour interval, optical transmission through the leaf is measured with the sensor and the absorbance of the ethanol extract is measured with the spectrophotometer set-up as illustrated in (c). A fiber-coupled AvaLight-DH-S-BAL light-source (Deuterium and halogen) shines a collimated beam through the solution (C1) in a UV-cuvette with 1 cm optical path. The transmitted beam is fed to an AvaSpec-ULS2048CL-EVO spectrometer (200–1100 nm) via a multi-mode 400 μm core optical fiber.

C2 = 2.5 %, C3 = 6.25 %, C4 = 12.5 %, and C5 = 25.0 %, as shown in Fig. 3(a). We label our solvent as C0 (c=0). The PD photocurrent $\Delta I_{\rm PD}$ (Δ represents that the dark current has been subtracted) is measured in air and in presence of a micro-droplet, which is transferred from each solution specimen with a hydrophilic tip of a ~100 μm core silica fiber. The droplets-on-chip have lateral diameters >500 μm, and hence covers the on-chip LED entirely (Fig. 1(c)), as was shown in our earlier work [31]. The same droplet is used to measure $\Delta I_{\rm PD}$ by driving the same LED in AM and FM operation at bias currents $I_{\rm LED}$ = 1–6 mA.

In the second experiment, we collect fresh green leaf specimens, one each from *Hamamelis virginiana* L. and *Capsicum annuum* L. plants. The leaves are then washed with demi water and wiped dry to remove dust and impurities from the surface. The PD photocurrent is then measured with the set-up described above, with the adaxial surface of the fresh leaf facing the on-chip LED (Fig. 1(c)). Each leaf is inserted into a vial containing 12 mL of ethanol at 300 K. The ethanol treatment emulates Chl stress in the leaf as the photosynthetic pigments dissolve in ethanol. After time t = 2, 4, 6, 8, and 10 hours, the leaf is withdrawn from its vial (Fig. 3(b)) and the corresponding PD photocurrent is measured. At each timestamp, the ethanolic extract is also sampled to measure its spectral absorbance with a hybrid spectrophotometer set-up illustrated in Fig. 3(c). This set-up consists of a fiber-coupled AvaLight-DH-S-BAL light source (Deuterium plus halogen) that shines a collimated beam through a UV-cuvette containing the test solution with 1 cm optical path. The transmitted beam is fed to an AvaSpec-ULS2048CL-EVO spectrometer (200–1100 nm) via a multi-mode 400 μm core optical fiber.

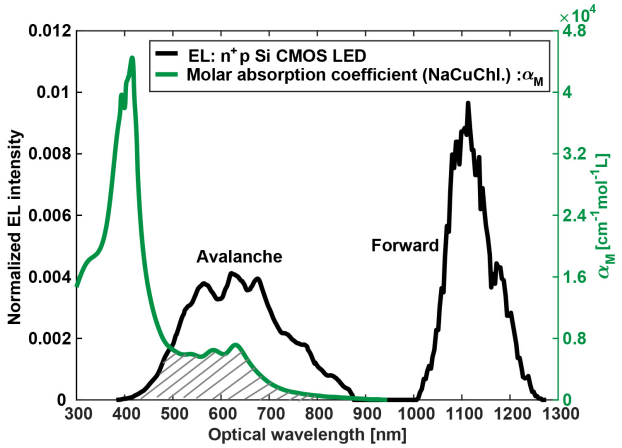

Fig. 4. Avalanche-mode (400–900 nm) and forward-mode (1000–1270 nm) normalized electroluminescent intensity spectra of the Si LED (in black) measured with a ADC-1000-USB and AvaSpec-UV/VIS/NIR spectrometers respectively from Avantes B.V. The measured molar absorption coefficient spectrum (in green) of NaCuChl in glycerol is measured with the hybrid spectrophotometer set-up shown in Fig. 3(c), and calibrating the value at λ = 626 nm from [2].

III. Results and Analysis

A. LED EL-Spectra and NaCuChl Molar Absorption Coefficient

Light emission from forward-biased Si diodes at λ in the range 1000–1270 nm, results from indirect (phonon-assisted) recombination of electron-hole pairs near the band-edge [20]. When the diode is reverse biased above the avalanche breakdown voltage, the high electric field in the depletion region accelerates the charge carriers to energies exceeding the bandgap of 1.12 eV. This leads to high-energy inter-band electronic transitions, resulting in a broad-spectrum EL peaking in the 600–700 nm wavelength window [22], [23], [25]. Fig. 4 shows the normalized EL spectra of the n^+p junction LED [27], [31] measured in avalanche-mode (AM) and forward-mode (FM) operation, with a UV/VIS (ADC-1000-USB) and AvaSpec-NIR spectrometer from Avantes B.V., respectively. The power normalized EL spectral irradiance $\varepsilon(\lambda)$ [nm^{-1}]is defined by:

$$\varepsilon(\lambda) = \frac{E(\lambda)}{\int_\lambda E(\lambda) \cdot {\rm d}\lambda}, \tag{1}$$

where $E(\lambda)$ is the measured EL intensity, and integration limits are from λ = 400 nm till λ = 900 nm. The AM EL spectrum has a significant overlap with the absorption spectrum of NaCuChl, whereas the same chemical absorbs negligibly in the FM EL spectrum of the Si LED. Fig. 4 also shows the molar absorption coefficient $\alpha_{\rm M}(\lambda)$ of our NaCuChl solution in glycerol. The specimen C1 ($c_1/c_{\rm ref}$ = 0.01) is used for this purpose and the absorbance $A(\lambda)$ is measured with the spectrophotometer set-up. The absorption coefficient of the specimen C1, $\alpha_{\rm C1}(\lambda)$ [cm^{-1}] is calculated from Beer-Lambert's law as:

$$\alpha_{\rm C1}(\lambda) = -\frac{\ln(1 - A_{\rm C1}(\lambda))}{L_{\rm opt}}, \tag{2}$$

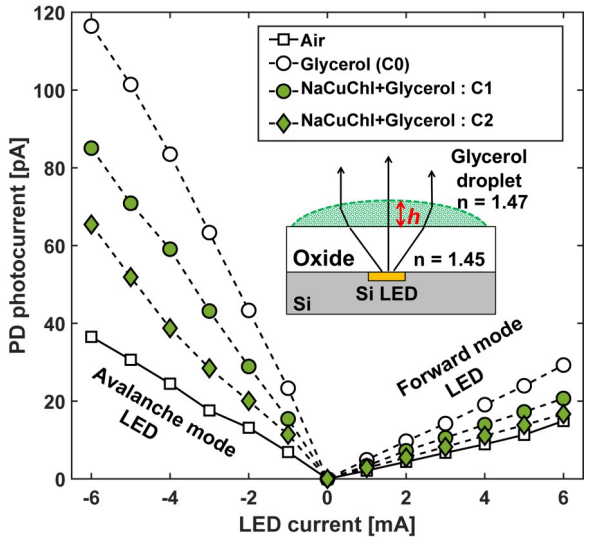

Fig. 5. Photocurrent (at reverse bias of 1 V) in the Si PD versus LED current in avalanche (−X axis) and forward (+X axis) modes of operation in air (squares), in presence of glycerol droplets from specimens C0 (white circles), C1 (green circles) and C2 (green diamonds). (Inset): Schematic cross-section showing the light-rays being focused by the plano-convex micro-lens formed by the droplet.

where $L_{\text{opt}} = 1$ cm is the optical path length of the light beam in the cuvette (see Fig. 3(c)). Subsequently, $\alpha_{\text{M}}(\lambda)$ [$\text{cm}^{-1}\text{mol}^{-1}\text{L}$] is estimated as:

$$\alpha_{\text{M}}(\lambda) = \left(\frac{c_{\text{ref}}}{c_1}\right) \cdot \left(\frac{\alpha_{\text{C1}}(\lambda)}{\alpha_{\text{C1}}(626\text{nm})}\right) \cdot 7192 \tag{3}$$

where we have used the literature reported molar absorption coefficient of NaCuChl as 7192 $\text{cm}^{-1}\text{mol}^{-1}\text{L}$ at $\lambda = 626$ nm (Q-band) [2] as a calibration point.

In order to use the Si LED as the light source for optical transmission measurements, we first compute the LED-specific molar absorption coefficient $\alpha_{\text{M}}^{\text{LED}}$ [$\text{cm}^{-1}\text{mol}^{-1}\text{L}$], and is expressed as:

$$\alpha_{\text{M}}^{\text{LED}} = \int_{\lambda} \alpha_{\text{M}}(\lambda) \cdot \varepsilon(\lambda) \cdot \text{d}\lambda, \tag{4}$$

where the limits of integration are the same as in eq. (1). We obtain $\alpha_{\text{M}}^{\text{LED}} = 4782.7$ $\text{cm}^{-1}\text{mol}^{-1}\text{L}$. Note that $\alpha_{\text{M}}^{\text{LED}}$ is a quantitative way to express the overlap between the $\varepsilon(\lambda)$ and $\alpha_{\text{M}}(\lambda)$ (indicated by the shaded region in Fig. 4).

B. Sodium Copper Chlorophyllin in Glycerol-Droplet

Fig. 5 shows the measured PD photocurrent (at a reverse bias of 1 V) which varies linearly with I_{LED} in both AM and FM LED operation, showing a linear relationship between optical power and I_{LED}. We observe that $\Delta I_{\text{PD}}^{\text{AM}} > \Delta I_{\text{PD}}^{\text{FM}}$ at any given I_{LED}. This is primarily due to the higher PD quantum efficiency for light emitted in AM operation [27]. Further, we observe that both $\Delta I_{\text{PD}}^{\text{AM}}$ and $\Delta I_{\text{PD}}^{\text{FM}}$ are, respectively, a factor of ∼3.2 and ∼2.0 higher in presence of the glycerol droplet (C0) as compared to transmission in air. This is explained by two factors. Firstly, there is a good refractive index matching between glycerol (n ≈ 1.47) and SiO_2 (n ≈ 1.45) over the droplet-covered die area. Secondly, the droplet acts as a plano-convex lens leading to a gain in the optical extraction efficiency (see inset of Fig. 5). A mismatch in the optical extraction efficiency between AM and FM operation is likely due to possible electrostatic effects on the shape or on the refractive index [39] of the glycerol droplet at widely different values of LED bias voltages: ∼19 V for AM and ∼1 V for FM LED. Since the pigment absorption window overlaps only with the AM EL spectrum, we can express the photocurrent in presence of the droplet for FM and AM LED operation, respectively as

$$\Delta I_{\text{PD(Gly)}}^{\text{FM}}(c_i) = \eta_{\text{LED}}^{\text{FM}} \cdot \eta_{\text{PD}}^{\text{FM}} \cdot \eta_{\text{Gly}}^{\text{FM}} \cdot I_{\text{LED}} \tag{5}$$

$$\Delta I_{\text{PD(Gly)}}^{\text{AM}}(c_i) = \eta_{\text{LED}}^{\text{AM}} \cdot \eta_{\text{PD}}^{\text{AM}} \cdot \eta_{\text{Gly}}^{\text{AM}} \cdot I_{\text{LED}} \cdot \exp[-\alpha(c_i) \cdot h] \tag{6}$$

where h is the droplet height, and c_i represents the concentration of the ith solution (i=0, 1, 2, 3, 4, 5). Here η_{LED} and η_{PD} represent the external quantum efficiencies of light-emission from the LED and light-detection by the PD, respectively. η_{Gly} is the light-extraction efficiency from the chip through the droplet. Considering a measurement error of ± 2 pA in the photocurrent, we observe in Fig. 5 that for droplets containing NaCuChl., absorption of visible light by the pigment leads to a decrease in $\Delta I_{\text{PD}}^{\text{AM}}$, as compared to transmission via the pure glycerol droplet. Small discrepancies in $\Delta I_{\text{PD}}^{\text{FM}}$ among droplet specimens are likely due to uncertainties in the droplet height and coverage area of the droplet, as was also observed in our earlier work [31].

Dividing eq. (6) by (5), we obtain the color ratio (COR) of optical coupling in AM to FM as:

$$\begin{aligned}\text{COR}(c_i) &= \left(\frac{\Delta I_{\text{PD(Gly)}}^{\text{AM}}(c_i)}{\Delta I_{\text{PD(Gly)}}^{\text{FM}}(c_i)}\right) \\ &= \left(\frac{\Delta I_{\text{PD(Gly)}}^{\text{AM}}(c_0)}{\Delta I_{\text{PD(Gly)}}^{\text{FM}}(c_0)}\right) \cdot \exp[-\alpha(c_i) \cdot h] \\ &= \text{COR}(c_0) \cdot \exp[-\alpha(c_i) \cdot h]\end{aligned} \tag{7}$$

where $\alpha(c_i) = \alpha_{\text{M}}^{\text{LED}} \cdot c_i$ is the effective absorption coefficient of the solution Ci from which the droplet is sampled, and c_0 represents pure glycerol (hence, $\alpha = 0$). Fig. 6 shows the measured COR versus relative concentration c/c_{ref}. The values are averaged over the set with $I_{\text{LED}} = [1, 2, 3, 4, 5, 6]$ mA. We observe that COR decreases with increasing c in accordance with Beer-Lambert law ($\propto \exp[-\alpha \cdot h]$). An exponential fit (least-squares method) yields the attenuation constant $\beta = 1.495$. Thus, we obtain the concentration of the target solution c_{ref} as

$$c_{\text{ref}} = \frac{\beta}{h \cdot \alpha_{\text{M}}^{\text{LED}}} \tag{8}$$

The droplet height h is estimated from optical microscopy as shown in Fig. 7(a). For droplets of size ranging from ∼100 μm – ∼1 mm, h is primarily governed by the angle of contact [40], [41] at the local liquid-chip (SiO_2) interface and the surface tension. Both parameters have uncertainties due to local surface properties and impurities (including the pigment) in the solvent. This results in a statistical variation in h, which is captured in Fig. 7(b) by analyzing multiple glycerol

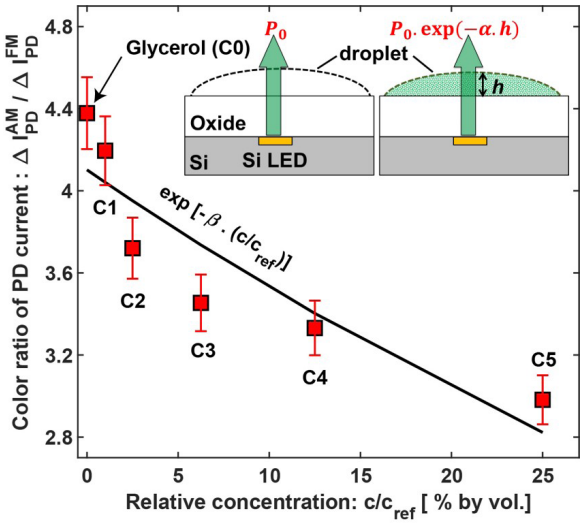

Fig. 6. Color ratio (AM to FM operation of the Si CMOS LED) of the PD photocurrent when light transmission occurs through the micro-droplets sampled from solution specimens C0 to C5. The values for COR are averaged over I_{LED} = 1–6 mA. COR decreases exponentially with increasing c (black solid line). The fitted attenuation constant $\beta = (\alpha_{ref}^{LED} \cdot h)$ is a function of the effective absorption coefficient of the reference NaCuChl. solution, and the droplet height h (see inset).

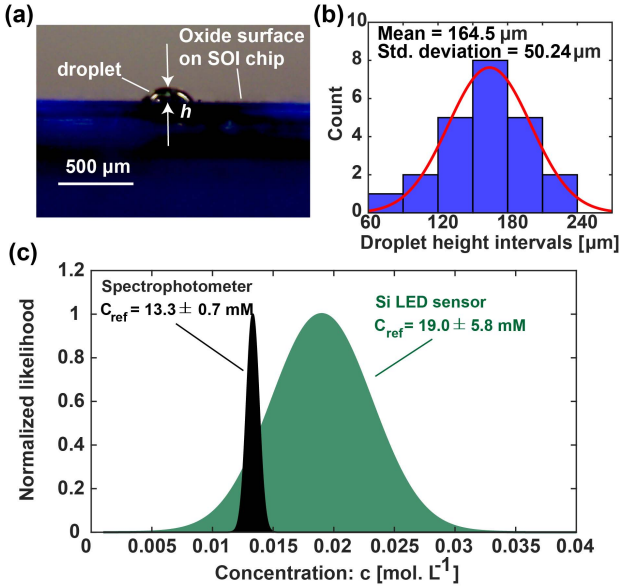

Fig. 7. (a) Optical micrograph of the side-view of a droplet-on-chip sampled from solution C3 showing the height profile. The estimated volume of the droplet was ~0.1 μL. (b) Histogram showing the mean and standard deviation in the measured center-height of different droplets transferred to the chip with a silica fiber tip. (c) Estimated concentration of the target NaCuChl solution (c_{ref}) via the Si LED based sensor (green) and via the hybrid spectrophotometer (black). The standard error of the Gaussian curves represents the uncertainty in experiment, while the mean represents the estimated value.

droplets on multiple dies. We observe $h = 164.50 \pm 50.24$ μm, where the error represents the standard deviation under a uni-modal Gaussian fit. Hence, using eq. (8) we obtain $c_{ref} = 19.0 \pm 5.8$ mmol.L^{-1} (mM). Fig. 7(c) shows this result graphically with a Gaussian likelihood curve, where the error in our estimation is represented by the standard deviation (σ).

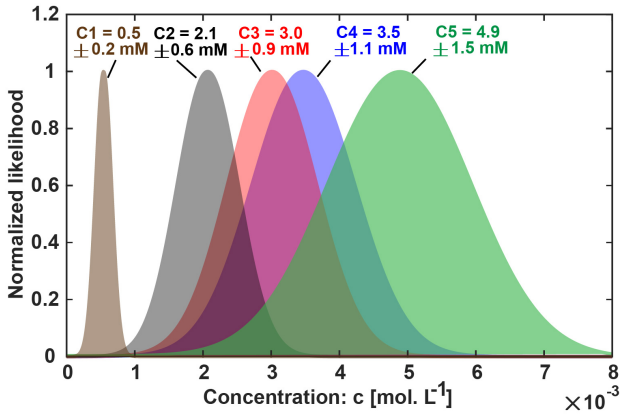

Fig. 8. Estimated concentrations of the diluted NaCuChl solution specimens C1–C5 via the Si LED based sensor, represented by a Gaussian likelihood curve. The standard error of the Gaussian curves represents the uncertainty in experiment, while the mean represents the estimated value.

We validate the estimated c_{ref}, by an independent absorbance measurement on the specimen C1, using the hybrid spectrophotometer (SP) set-up as:

$$c_{ref}^{SP} = \left(\frac{\alpha_{C1}(626nm)}{\alpha_M(626nm)}\right) \cdot \left(\frac{c_{ref}}{c_1}\right) \tag{9}$$

where $\alpha_{C1}(626nm)$ is obtained from eq. (2). This gives $c_{ref}{}^{SP} = 13.3 \pm 0.7$ mmol.L^{-1} (mM), which is in a close agreement with that obtained by our droplet sensing method with the broad-band Si LED. A small positive deviation in the estimated value with our sensor is likely due to an under-estimation of α_M^{LED}, where we have ignored the contribution of the weak absorption tail of NaCuChl for $\lambda > 900$ nm in eq. (4). Error could also arise due to possible inhomogeneities in the diluted specimens (high viscosity of glycerol).

For specimens C1 to C5, the concentrations can also be obtained independently using eq. (7) as

$$c_i = \left(\frac{1}{h \cdot \alpha_M^{LED}}\right) \cdot \left(-\ln\left[\frac{COR(c_i)}{COR(c_0)}\right]\right) \tag{10}$$

which yields $c_1 = 0.5 \pm 0.2$ mM, $c_2 = 2.1 \pm 0.6$ mM, $c_3 = 3.0 \pm 0.9$ mM, $c_4 = 3.5 \pm 1.1$ mM, and $c_5 = 4.9 \pm 1.5$ mM, as shown graphically in Fig. 8. Note that the standard error in the estimations propagates predominantly from the error in h. Taking the 1st order derivative approximation of eq. (10), we get $\delta c_i = c_i \cdot (\delta h / h)$. Consequently, the absolute error is proportional to the concentration c_i. In order to evaluate the sensitivity $S_{droplet}$ of our sensor, we apply the differential approximation to eq. (7) that gives us

$$S_{droplet} = \frac{\delta COR(c_i)}{\delta c_i} = -COR(c_i) \cdot \alpha_M^{LED} \cdot h \tag{11}$$

where the minus sign indicates that COR decreases with increasing c. At low concentrations, e.g. for specimen C1, we obtain $|S_{droplet}| = 330$ mol^{-1}L.

C. Non-Invasive Sensing of Chl. Deficiency in Leaves

Chlorophyll (Chl. a,b) and carotenoids (β-carotene) are the two naturally occurring dominant photosynthetic pigments [6],

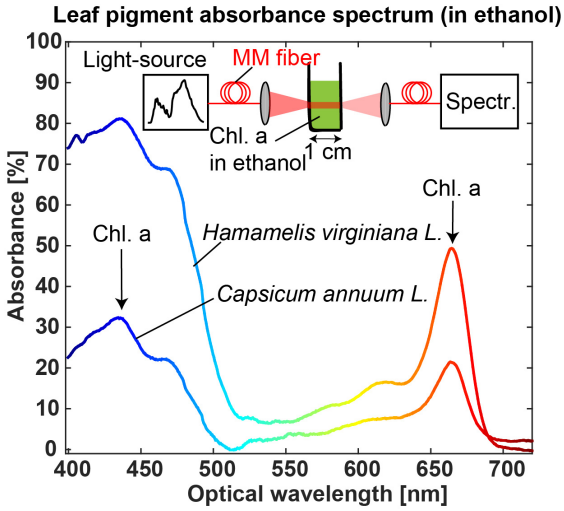

Fig. 9. Measured spectral absorbance of ethanolic solutions of photosynthetic pigments extracted from *Hamamelis* and *Capsicum* leaf samples, treated with 12 mL ethanol for 2 hours at 300 K. The peak at $\lambda \approx 660$ nm is a signature of Chl. a, while the local peak at $\lambda \approx 475$ nm indicates the presence of carotenoids. (Inset): Hybrid spectrophotometer set-up used for the absorbance measurement.

crucial for the growth and nutrition in plants. Reduction of Chl in leaves (chlorosis) is an important marker of plant stress. The measured absorbance (A) spectra of pigments extracted (in ethanol) from leaves of two example species, namely *Capsicum annuum* L. and *Hamamelis virginiana* L., are shown in Fig. 9. The ethanolic extracts were sampled after a duration of 2 hours of dissolution at 300 K, and analyzed with the hybrid spectrophotometer set-up (see inset). Both spectra exhibit peaks at $\lambda_R \approx 660$ nm, $\lambda_B \approx 475$ nm, and $\lambda_V \approx 430$ nm. The peaks at λ_R and λ_V are attributed to Chl. a, and the peak at λ_B is a signature of β-carotene [6], where small deviations (± 5 nm) [42] in peak positions may occur due to different solvents used. We observe that the AM EL spectrum of the Si LED has a maximum overlap with the absorption of Chl. a, followed by a relatively smaller overlap with that of carotene.

The COR was measured for the *Capsicum* and *Hamamelis* leaves at different timestamps of ethanol treatment. This was done by placing the leaves on top of the Si CMOS LED in our sensor and measuring light transmission through the leaf. The COR in the PD photocurrent against the measured absorbance of the corresponding ethanolic extract sampled immediately after withdrawing the *Capsicum* and *Hamamelis* leaf from the vial, are shown in Fig. 10(a) and (b), respectively. Also shown in the same figure are the corresponding Chl. a concentrations (c) (in solution) calculated from measured A(660 nm) and the literature-reported [43]–[45] $\alpha_{M(ChlA)}$(660 nm) of 32640 $cm^{-1}mol^{-1}L$. We observe a linear relationship (high correlation) between the COR and A. This is expected because the total amount of pigment molecules is conserved during the physical dissolution process. Hence, as the optical transmission through the leaf increases, the [Chl. a] in solution increases. The slope of the linear fit gives us $\delta COR/\delta A[\%] = 0.024$ and 0.0325 for *Capsicum*

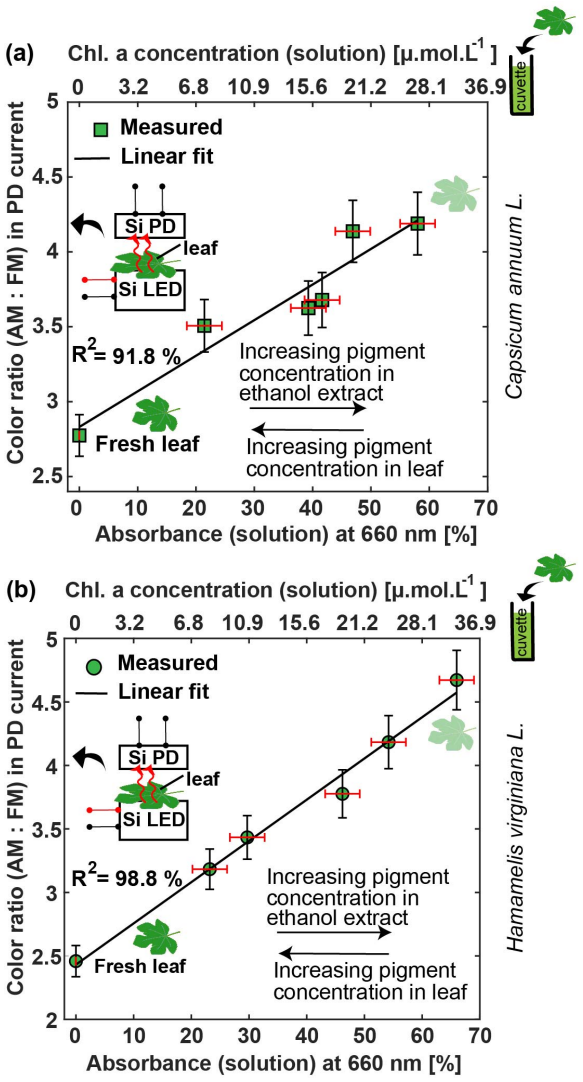

Fig. 10. COR (for the leaf) versus 660 nm absorbance (in ethanolic solution) for (a) *Capsicum* and (b) *Hamamelis* leaf samples with indicated error bars (symbols). The COR was measured by placing the leaf on the Si CMOS LED (see inset). The black solid line represents the linear fit, with a slope representing the mean sensitivity ($\delta COR/\delta A[\%]$). The top X-axis maps the absorbance to the equivalent Chl. a concentration by using $\alpha_{M(ChlA)}(660\text{ nm}) = 32640\ cm^{-1}mol^{-1}L$.

and *Hamamelis* respectively. Considering an error margin of ± 0.2 in the COR (measured through the leaf), we obtain a resolution (and hence the detection limit) of absorbance $\delta A_{res}[\%]$ of ≈ 8.3 % and ≈ 6.2 % for the *Capsicum* and *Hamamelis* leaf respectively. Further, using a differential approximation of eq. (2), we can calculate the detection limit in terms of concentration (in solution) c as:

$$\delta c_{res} = \left(\frac{1}{\alpha_{M(ChlA)} \cdot L_{opt}}\right) \cdot \left(\frac{\delta A_{res}}{100 - A[\%]}\right) \qquad (12)$$

Thus, we obtain $\delta c_{res} \approx 5\ \mu M$ for *Capsicum* and $\approx 3.8\ \mu M$ for *Hamamelis* respectively, for a reference value of $A = 50\%$ (in solution), and $L_{opt} = 1$ cm (path length in cuvette).

Further we can define the mean sensitivity (S_{leaf}) of our sensor as

$$S_{\text{leaf}} = \frac{\delta \text{COR}}{\delta(c_{\text{ChlA}})} = \frac{\delta \text{COR}}{\delta A[\%]} \cdot \frac{\delta A[\%]}{\delta(c_{\text{ChlA}})} = \left(\frac{\delta \text{COR}}{\delta A[\%]}\right) \cdot \alpha_{\text{M(ChlA)}} \cdot L_{\text{opt}} \cdot (100 - A[\%]) \quad (13)$$

where A is obtained by rearranging eq. (2) as $100\times[1 - \exp(-\alpha_{\text{M(ChlA)}} \cdot L_{\text{opt}} \cdot \Delta n_{\text{ChlA}}/V_{\text{sol}})]$. S depends on Δn_{ChlA}. Substituting values, we obtain $S_{\text{leaf}} = 3.9\times10^4$ mol^{-1}L and 5.3×10^4 mol^{-1}L for the *Capsicum* and the *Hamamelis* leaf, respectively, for a reference $A = 50\%$. Differences in S between the two leaf species obtained by this method is due to sample-to-sample variation. This can be attributed to the different optical paths through the different cellular arrangements in the inner mesophyll tissue of the two leaves, and the different spatial distribution of Chl.

IV. Discussion and Outlook

We have presented the first proof-of-concept small-volume ($\sim$0.1 μL) optical absorption sensor with broad-spectrum avalanche-mode Si LEDs in standard CMOS technology. The same LED emits light with two disjoint and bias-dependent EL-spectra, only one of which is absorbed by a target specimen. This obviates the need for modifications in fabrication process and material composition, which are typically employed in tailoring the efficiency and EL-wavelength of Si-based light sources, as summarized in Table I. We outline the performance, future scope and applicability of our sensor under the following headings:

A. Resolution and Sensitivity

In solution phase, the dominant source of error in c_{ref} in our experiment is the uncertainty in h, and thus, not limited by the LED or PD. For specimen C1 (the lowest concentration), we obtain a resolution of $\sim$200 μM (Fig. 8). If the droplet height is known precisely, then the error in our experiment will be dominated by the 4 % relative uncertainty in measuring COR(c_i). Using eq. (10), we then obtain that $\delta c_1/c_1$ to be $\sim$8 %. This amounts to an absolute error of 40 μM. Increasing the precision of the dispensed volume of the micro-droplet is envisaged in future developments, which will reduce the error and hence increase the resolution towards state-of-the-art ($\sim$1 μM) [46], [47] that uses hybrid quasi-monochromatic LEDs with III-V semiconductors in relatively bulky sensors.

Eqs. (11) indicates that at a given reference concentration, sensitivity is proportional to the optical path length through which absorption takes place. In the non-invasive detection via a leaf, we emulate Chl stress by systematic reduction in the photosynthetic pigments via the ethanol treatment. The inner micro-structure of a leaf is largely a matrix of loosely packed mesophyll cells with a certain fraction of inter-cellular voids [48]. Light from the Si LED propagates through these mesophyll cells in a diffuse manner (multiple Fresnel reflections at the cell-void interfaces) [49], [50] before emerging into air and being collected by the photodiode. The light from the LED is divergent and hence it illuminates a patch of area $\sim$10 cm^2 on the leaf. The color ratio measured is therefore averaged out over this spot, which relaxes the constraints on precise alignment. Thus, the net optical path is folded by a large leaf-dependent factor. Hence, detection with the intact leaf is expected to yield a higher sensitivity, as compared to the measurement in solution. The only trade-off in using a leaf directly is the inclusion of local variations in pigment distribution and optical path length through the leaf tissue in a single leaf.

B. Stability

Glycerol, being a low-voltatile (boiling points > 400 K) [51], polar and organic solvent, is a suitable choice for the medium to dispense stable micro-droplets. The back-end oxide layer in the CMOS chip provides good passivation to shield the Si LED from chemicals in the droplet. Post-removal of droplet with iso-propanol, the chip surface was re-used for the next droplet with negligible change in ΔI_{PD}. However, only the Al-capped bond pads limit the degree of re-usability of the sensor in solution-phase due to possible (electro-)chemical side-reactions with and glycerol [52], [53] and water. For sensing carmine [31], the same device could be re-used for upto 6 droplet specimens, while for NaCuChl upto 3 droplets could be measured, before the Al-capping was corroded. For a given droplet, the measurements shown in Fig. 5 were stable for at least $\sim$5-7 minutes. Longer duration of LED operation resulted in reactions between the Al-capped bond pads and glycerol, which in turn affects the shape of the droplet and pigment homogeneity.

C. Device Footprint and Power Consumption

With the exception of the off-chip Si PD, our sensor has a footprint of less than $\sim$0.5 mm^2, which includes a dual-spectrum light-source within an area of $\sim$0.01 mm^2. For industrial CMOS technologies, the production costs for silicon are typically 10–50 eurocents per mm^2 of die area. So, the cost of a single Si LED is estimated to be within a eurocent. Monolithic integration of the Si PD with a dedicated layout will further reduce the form factor of the sensor, which will be studied in our future work. From the viewpoint of field-implementation of such a sensor, either open-cavity or glass-lid packaging would be preferred. In the latter scenario, an additional $\sim$7 % loss in optical power is expected due to reflections at the air-glass interfaces. The dc power consumption in our LED ranged from 18 mW ($I_{\text{LED}} = 1$ mA) till 118 mW ($I_{\text{LED}} = 6$ mA). For each I_{LED}, an integration time of $\sim$500 ms was used to reduce the noise in measuring the corresponding photocurrent with the SMU, leading to a minimum energy consumption of 10 mJ. In a prior work, the thermal resistance on the chip at a distance of 10 μm from the LED was extracted to be 35 K/W [27]. Thus, for an electrical input power of 20 mW, the increase in steady-state temperature due to self-heating in the LED is within 1 K. The CMOS technology is widely successful to provide high-level monolithic integration

TABLE I
PERFORMANCE COMPARISON OF Si-BASED LIGHT-EMITTING DEVICES IN LITERATURE

Light-emitter type type	Typical EL wavelength [nm]	Optical power efficiency [order of magnitude]	Standard CMOS compatibility	Wavelength selection	References
c-Si p-n junction (this work)	400–900 (avalanche) $\sim$ 1100 (forward)	10^{-3}–10^{-6}	Yes	By switching bias polarity	[19], [20], [24], [26]
Si-on-insulator FinFET technology	$\sim$ 1100	10^{-3}	No	Fixed	[54]
Si nanocrystals in SiO_2	700–900	10^{-3}	Yes	Fixed by fabrication process	[55], [56], [57]
Strained Si-Ge	1200–1600	10^{-2}	No	Fixed by stoichiometry	[58], [59], [60], [61]
Er-doped Si	1530–1540	10^{-3}	No	Fixed by fabrication process	[55], [62]

for electronic driver/read-out circuits. Pushing the limits of silicon based light sources, therefore, helps in miniaturizing such sensors and provide a low-cost alternative for coarse and rapid testing of food/water quality and plant health, where high precision is not critical.

V. CONCLUSION

We reported the first proof-of-principle of optical absorption sensing of pigment in solution with a broad-spectrum silicon micro LED designed in a standard silicon-on-insulator CMOS technology. Vertical optical transmission through a glycerol micro-droplet containing a chlorophyll based pigment (sodium copper chlorophyllin) was measured with a silicon photodiode. The on-chip silicon LED was driven in both forward and avalanche modes of operation, which steered its electroluminescent spectrum between visible and near-infrared, without replacing the droplet. The effective absorption coefficient and consequently the concentration in solution were determined from the color ratio (COR) of the measured photocurrent and the molar absorption coefficient of the pigment; the results were validated with a spectrophotometer. We validated our sensor further by employing it as a non-invasive chlorophyll sensor for stress monitor in plant leaves. Light emitted from the LED propagates through the leaf diffusely and undergoes absorption by the cellular chlorophyll before being detected by the photodiode. The COR of the photocurrent was shown to vary linearly with the decrease of chlorophyll from the leaf. Our work demonstrates the viability of a CMOS-integrated silicon LED, as a light source for micro-volume optical sensing.

ACKNOWLEDGMENT

The authors would like to thank NXP Semiconductors B.V. for silicon device fabrication. They thank Gideon Emmaneel, Rob Luttjeboer, and Xianfeng Chen from the department of Precision and Microsystems Engineering, TU Delft for technical support. They also thank Jurriaan Schmitz and Raymond J.E. Hueting from the University of Twente for permitting to use the silicon devices.

REFERENCES

[1] H. Scheer, "An overview of chlorophylls and bacteriochlorophylls: Biochemistry, biophysics, functions and applications," in *Chlorophylls and Bacteriochlorophylls* (Advances in Photosynthesis and Respiration), B. Grimm, R. J. Porra, W. Rüdiger, and H. Scheer, Eds., vol. 25. Dordrecht, The Netherlands: Springer, 2006, ch. 1, pp. 1–26.

[2] A. F. Uchoa, A. M. Konopko, and M. S. Baptista, "Chlorophyllin derivatives as photosensitizers: Synthesis and photodynamic properties," *J. Brazilian Chem. Soc.*, vol. 26, no. 12, pp. 2615–2622, 2015.

[3] D. Cui, M. Li, and Q. Zhang, "Development of an optical sensor for crop leaf chlorophyll content detection," *Comput. Electron. Agricult.*, vol. 69, no. 2, pp. 171–176, Dec. 2009.

[4] J. T. Alander, V. Bochko, B. Martinkauppi, S. Saranwong, and T. Mantere, "A review of optical nondestructive visual and near-infrared methods for food quality and safety," *Int. J. Spectrosc.*, vol. 2013, pp. 1–36, Mar. 2013.

[5] L. Zeng and D. Li, "Development of *in situ* sensors for chlorophyll concentration measurement," *J. Sensors*, vol. 2015, pp. 1–16, Jan. 2015.

[6] H. Croft and J. M. Chen, "Leaf pigment content," in *Comprehensive Remote Sensing*, S. Lian, Ed., vol. 3. Amsterdam, The Netherlands: Elsevier, ch. 9, 2018, pp. 117–142.

[7] S. Bergsträsser *et al.*, "HyperART: Non-invasive quantification of leaf traits using hyperspectral absorption-reflectance-transmittance imaging," *Plant Methods*, vol. 11, no. 1, p. 1, 2015.

[8] H. Gao, C. Yan, W. Wu, and J. Li, "Application of microfluidic chip technology in food safety sensing," *Sensors*, vol. 20, no. 6, p. 1792, Mar. 2020.

[9] M. O'Toole and D. Diamond, "Absorbance based light emitting diode optical sensors and sensing devices," *Sensors*, vol. 8, no. 4, pp. 2453–2479, Apr. 2008.

[10] F. M. Padilla, R. de Souza, M. T. Peña-Fleitas, M. Gallardo, C. Giménez, and R. B. Thompson, "Different responses of various chlorophyll meters to increasing nitrogen supply in sweet pepper," *Frontiers Plant Sci.*, vol. 9, p. 1752, Nov. 2018.

[11] G. Minas, J. C. Ribeiro, R. F. Wolffenbuttel, and J. H. Correia, "On-chip integrated CMOS optical detection microsystem for spectrophotometric analyses in biological microfluidic systems," in *Proc. IEEE Int. Symp. Ind. Electron. (ISIE)*, Jun. 2005, pp. 1133–1138.

[12] R. Soref, "Applications of silicon-based optoelectronics," *MRS Bull.*, vol. 23, no. 4, pp. 20–24, Apr. 1998.

[13] L. W. Snyman *et al.*, "Optical sources, integrated optical detectors, and optical waveguides in standard silicon CMOS integrated circuitry," *Proc. SPIE*, vol. 3953, pp. 20–36, Mar. 2000.

[14] U. Lu *et al.*, "CMOS chip as luminescent sensor for biochemical reactions," *IEEE Sensors J.*, vol. 3, no. 3, pp. 310–316, Jun. 2003.

[15] F. J. Blanco *et al.*, "Microfluidic-optical integrated CMOS compatible devices for label-free biochemical sensing," *J. Micromech. Microeng.*, vol. 16, no. 5, pp. 1006–1016, Apr. 2006.

[16] K. De Vos, I. Bartolozzi, E. Schacht, P. Bienstman, and R. Baets, "Silicon-on-insulator microring resonator for sensitive and label-free biosensing," *Opt. Exp.*, vol. 15, no. 12, pp. 7610–7615, Jun. 2007.

[17] A. Frey, M. Schienle, and H. Seidel, "CMOS based sensors for biochemical analysis," in *Proc. Int. Solid-State Sensors, Actuat. Microsyst. Conf.*, Jun. 2009, pp. 1670–1673.

[18] C. Sun *et al.*, "Single-chip microprocessor that communicates directly using light," *Nature*, vol. 528, no. 7583, pp. 534–538, Dec. 2015.

[19] K. Xu, Y. Chen, T. A. Okhai, and L. W. Snyman, "Micro optical sensors based on avalanching silicon light-emitting devices monolithically integrated on chips," *Opt. Mater. Exp.*, vol. 9, no. 10, pp. 3985–3997, Oct. 2019.

[20] M. Green, J. Zhao, A. Wang, P. J. Reece, and M. Gal, "Efficient silicon light emitting diodes," *Nature*, vol. 412, no. 6849, pp. 805–808, Aug. 2001.

[21] T. Trupke, J. Zhao, A. Wang, R. Corkish, and M. A. Green, "Very efficient light emission from bulk crystalline silicon," *Appl. Phys. Lett.*, vol. 82, no. 18, pp. 2996–2998, May 2003.

[22] A. G. Chynoweth and K. G. McKay, "Photon emission from avalanche breakdown in silicon," *Phys. Rev.*, vol. 102, no. 2, pp. 369–376, Apr. 1956.

[23] S. Dutta, R. J. E. Hueting, A.-J. Annema, L. Qi, L. K. Nanver, and J. Schmitz, "Opto-electronic modeling of light emission from avalanche-mode silicon p^+n junctions," *J. Appl. Phys.*, vol. 118, Sep. 2015, Art. no. 114506.

[24] L. W. Snyman, M. du Plessis, and H. Aharoni, "Injection-avalanche-based n^+pn silicon complementary metal-oxide-semiconductor light-emitting device (450–750 nm) with 2-order-of-magnitude increase in light emission intensity," *Jpn. J. Appl. Phys.*, vol. 46, no. 4B, pp. 2474–2480, Apr. 2007.

[25] L. W. Snyman and K. Xu, "Stimulation of 450, 650, and 850 nm optical emissions from custom designed silicon LED devices by utilizing carrier energy and carrier momentum engineering," *Proc. SPIE*, vol. 10036, Feb. 2017, Art. no. 1003603.

[26] S. Dutta, G. J. M. Wienk, R. J. E. Hueting, J. Schmitz, and A.-J. Annema, "Optical power efficiency versus breakdown voltage of avalanche-mode silicon LEDs in CMOS," *IEEE Electron Device Lett.*, vol. 38, no. 7, pp. 898–901, Jul. 2017.

[27] S. Dutta, V. Agarwal, R. J. E. Hueting, J. Schmitz, and A.-J. Annema, "Monolithic optical link in silicon-on-insulator CMOS technology," *Opt. Exp.*, vol. 25, no. 5, pp. 5440–5456, Mar. 2017.

[28] B. Huang *et al.*, "CMOS monolithic optoelectronic integrated circuit for on-chip optical interconnection," *Opt. Commun.*, vol. 284, nos. 16–17, pp. 3924–3927, Aug. 2011.

[29] V. Agarwal *et al.*, "Optocoupling in CMOS," in *IEDM Tech. Dig.*, Dec. 2018, pp. 739–742.

[30] I. Gorczyca, T. Suski, N. E. Christensen, and A. Svane, "Limitations to band gap tuning in nitride semiconductor alloys," *Appl. Phys. Lett.*, vol. 96, no. 10, Mar. 2010, Art. no. 101907.

[31] S. Dutta, P. G. Steeneken, and G. J. Verbiest, "Optical absorption sensing with dual-spectrum silicon LEDs in SOI-CMOS technology," in *Proc. IEEE SENSORS*, Oct. 2020, p. 6498.

[32] P. Wessels *et al.*, "Advanced BCD technology for automotive, audio and power applications," *Solid-State Electron.*, vol. 51, no. 2, pp. 195–211, Feb. 2007.

[33] E. R. Hunt, Jr., B. N. Rock, and P. S. Rock, "Measuring of leaf water content by infrared reflectance," *Remote Sens. Environ.*, vol. 22, no. 3, pp. 429–435, Aug. 1987.

[34] H. W. Gausman, W. A. Allen, and D. E. Escobar, "Refractive index of plant cell walls," *Appl. Opt.*, vol. 13, no. 1, pp. 109–111, Jan. 1974.

[35] A. Bricaud, A. Morel, and L. Prieur, "Absorption by dissolved organic matter of the sea (yellow substance) in the UV and visible domains1," *Limnol. Oceanogr.*, vol. 26, no. 1, pp. 43–53, Jan. 1981.

[36] G. Pérez, C. Queimaliños, E. Balseiro, and B. Modenutti, "Phytoplankton absorption spectra along the water column in deep North Patagonian Andean lakes (Argentina)," *Limnologica*, vol. 37, no. 1, pp. 3–16, Feb. 2007.

[37] Z. Lee and K. L. Carder, "Absorption spectrum of phytoplankton pigments derived from hyperspectral remote-sensing reflectance," *Remote Sens. Environ.*, vol. 89, no. 3, pp. 361–368, Feb. 2004.

[38] M. Nitzan, A. Romem, and R. Koppel, "Pulse oximetry: Fundamentals and technology," *Med. Devices, Evidences Res.*, vol. 2014, no. 7, pp. 231–239, Jul. 2014.

[39] H. Kanemaru, S. Yukita, H. Namiki, Y. Nosaka, T. Kobayashi, and E. Tokunaga, "Giant pockels effect of polar organic solvents and water in the electric double layer on a transparent electrode," *RSC Adv.*, vol. 7, no. 72, pp. 45682–45690, 2017.

[40] A. Moldovan *et al.*, "Wetting properties of glycerol on silicon, native SiO_2, and bulk SiO_2 by scanning polarization force microscopy," *J. Adhes. Sci. Technol.*, vol. 28, no. 13, pp. 1277–1287, Mar. 2014.

[41] F. Behroozi and P. S. Behroozi, "Reliable determination of contact angle from the height and volume of sessile drops," *Amer. J. Phys.*, vol. 87, no. 1, pp. 28–32, Jan. 2019.

[42] G. R. Seely and R. G. Jensen, "Effect of solvent on the spectrum of chlorophyll," *Spectrochimica Acta*, vol. 21, no. 10, pp. 1835–1845, Oct. 1965.

[43] H. H. Strain, M. R. Thomas, and J. J. Katz, "Spectral absorption properties of ordinary and fully deuteriated chlorophylls a and b," *Biochimica Biophysica Acta*, vol. 75, pp. 306–311, Jan. 1963.

[44] H. K. Lichtenthaler, "Chlorophylls and carotenoids: Pigments of photosynthetic biomembranes," in *Methods in Enzymology* (Plant Cell Membranes), L. Packer and R. Douce, Eds., vol. 148. New York, NY, USA: Academic, 1987, ch. 34, pp. 350–382.

[45] H. Du, R.-C.-A. Fuh, J. Li, L. A. Corkan, and J. S. Lindsey, "PhotochemCAD: A computer-aided design and research tool in photochemistry," *Photochem. Photobiol.*, vol. 68, no. 2, pp. 141–142, Aug. 1998.

[46] M. O'Toole, K. T. Lau, R. Shepherd, C. Slater, and D. Diamond, "Determination of phosphate using a highly sensitive paired emitter–detector diode photometric flow detector," *Analytica Chim. Acta*, vol. 597, no. 2, pp. 290–294, Aug. 2007.

[47] J. Huang, "A dual-wavelength light-emitting diode based detector for flow-injection analysis process analysers," *Talanta*, vol. 39, no. 6, pp. 589–592, Jun. 1992.

[48] H. W. Gausman, W. A. Allen, R. Cardenas, and A. J. Richardson, "Relation of light reflectance to histological and physical evaluations of cotton leaf maturity," *Appl. Opt.*, vol. 9, no. 3, pp. 545–552, Mar. 1970.

[49] E. A. Walter-Shea and J. M. Norman, "Leaf optical properties," in *Photon-Vegetation Interactions*, R. B. Myneni and J. Ross, Eds., vol. 8. Berlin, Germany: Springer, ch. 8, 1991, pp. 229–251.

[50] J. T. Woolley, "Reflectance and transmittance of light by leaves," *Plant Physiol.*, vol. 47, no. 5, pp. 656–662, May 1971.

[51] L. B. Lane, "Freezing points of glycerol and its aqueous solutions," *Ind. Eng. Chem.*, vol. 17, no. 9, p. 924, Sep. 1925.

[52] H. B. Zhang, J. H. Yang, F. Gao, and J. J. Lin, "Experimental study of the breakdown characteristic of glycerol as energy storage medium in pulse forming line," in *Proc. Annu. Rep. Conf. Electr. Insul. Dielectr. Phenomena*, Oct. 2013, pp. 850–853.

[53] S. Schünemann, F. Schüth, and H. Tüysüz, "Selective glycerol oxidation over ordered mesoporous copper aluminum oxide catalysts," *Catal. Sci. Technol.*, vol. 7, no. 23, pp. 5614–5624, 2017.

[54] G. Piccolo, P. I. Kuindersma, L.-A. Ragnarsson, R. J. E. Hueting, N. Collaert, and J. Schmitz, "Silicon LEDs in FinFET technology," in *Proc. 44th Eur. Solid State Device Res. Conf. (ESSDERC)*, Sep. 2014, pp. 274–277.

[55] L. Pavesi, "Silicon-based light sources for silicon integrated circuits," *Adv. Opt. Technol.*, vol. 2008, pp. 1–12, Jun. 2008.

[56] L. Pavesi, L. D. Negro, C. Mazzoleni, G. Franzò, and F. Priolo, "Optical gain in silicon nanocrystals," *Nature*, vol. 408, no. 6811, pp. 440–444, Nov. 2000.

[57] R. J. Walters, G. I. Bourianoff, and H. A. Atwater, "Field-effect electroluminescence in silicon nanocrystals," *Nature Mater.*, vol. 4, no. 2, pp. 143–146, Jan. 2005.

[58] J. Liu *et al.*, "Tensile-strained, n-type Ge as a gain medium for monolithic laser integration on Si," *Opt. Exp.*, vol. 15, no. 18, pp. 11272–11277, Sep. 2007.

[59] B. Schwartz, A. Klossek, M. Kittler, M. Oehme, E. Kasper, and J. Schulze, "Electroluminescence of germanium LEDs on silicon: Influence of antimony doping," *Phys. Status Solidi C*, vol. 11, nos. 11–12, pp. 1686–1691, Oct. 2014.

[60] M. Kaschel, M. Schmid, M. Gollhofer, J. Werner, M. Oehme, and J. Schulze, "Room-temperature electroluminescence from tensile strained double-heterojunction germanium pin LEDs on silicon substrates," *Solid-State Electron.*, vol. 83, pp. 87–91, May 2013.

[61] H. Li *et al.*, "Silicon waveguide integrated with germanium photodetector for a photonic-integrated FBG interrogator," *Nanomaterials*, vol. 10, no. 9, p. 1683, Aug. 2020.

[62] N. Daldosso *et al.*, "Er-coupled Si nanocluster waveguide," *IEEE J. Sel. Topics Quantum Electron.*, vol. 12, no. 6, pp. 1607–1617, Nov. 2006.

Satadal Dutta received the B.Tech. (Hons.) degree in electronics and electrical communication engineering and the M.Tech. degree in microelectronics and VLSI from IIT Kharagpur, Kharagpur, India, in 2013, and the Ph.D. degree from the MESA+ Institute for Nanotechnology, University of Twente, Enschede, The Netherlands, in November 2017. From 2018 to 2019, he worked as a Photonics Design Engineer with LioniX International B.V. Since April 2019, he has been a Postdoctoral Fellow with the Department of Precision and Microsystems Engineering, Delft University of Technology. His primary research interests include optoelectronics, integrated optics, and silicon CMOS technology, with 20 peer reviewed journals and conference publications till date. He is currently working under the Plantenna Research Program, focused on developing new ultrasound and optical sensors for plant-health monitoring, and holds one patent application.

Peter G. Steeneken received the M.Sc. and Ph.D. degrees in experimental solid state physics from the University of Groningen, The Netherlands. In 2002, he joined Philips Research and NXP Research in Eindhoven, as an Industrial Scientist focusing on the modeling, characterization and reliability of CMOS MEMS devices for sensors, actuators, and RF applications. Since 2013, he has been a Professor of Applied Nanophysics with the Kavli Institute of Nanoscience, Delft, The Netherlands. Since 2017, he has been a Full Professor with TU Delft's Precision and Microsystems Engineering Department, chairing the section Dynamics of Micro and Nanosystems. He currently leads the sensors workpackage of the Graphene Flagship and the large national project Plantenna on plant-based sensor technology. He has authored more than 100 journals and conference publications and holds 44 granted U.S. patents. His research focuses on bridging the gap between fundamental physics and applications, with a focus on high frequency nanomechanical sensor devices.

Gerard J. Verbiest received the M.Sc. *(cum laude)* degree in theoretical physics and the Ph.D. degree in experimental surface science from the Leiden University, The Netherlands, in 2009 and 2013, respectively. In 2013, he joined the RWTH Aachen, Germany, as a Postdoctoral Researcher, where he working on the dynamics and charge transport as a function of strain in suspended graphene membranes with aim to develop new sensors. Since 2018, he has been an Assistant Professor (tenure track) with TU Delft's Precision and Microsystems Engineering Department as part of the section Dynamics of Micro and Nanosystems. He has authored more than 24 journals and conference publications and holds six patent applications. His research focuses on nano acoustic sensing. He is currently working on subsurface atomic force microscopy, heat, and phonon transport in 2D materials, and plant-based sensor technology.